Assessment of resolution and accuracy of the Moving Window Cross Spectral technique for monitoring crustal temporal variations using ambient seismic noise.

Daniel Clarke, Lucia Zaccarelli, N.M. Shapiro, Florent Brenguier

submitted to *Geophys. J. Int.*

Assessment of resolution and accuracy of the Moving Window Cross Spectral technique for monitoring crustal temporal variations using ambient seismic noise

D. Clarke[1⋆], L. Zaccarelli[1], N. M. Shapiro[1], F. Brenguier[2]

[1] *Institut de Physique du Globe de Paris, Sorbonne Paris Cité, CNRS (UMS7154), 1 rue Jussieu,* 75238 *Paris, cedex 5, Fran*

[2] *Observatoire Volcanologique du Piton de la Fournaise, 14 RN3 - Km 27,* 97418*, La Plaine des Cafres, Ile de La Réunion,*

19 April 2011

SUMMARY

Temporal variations in the elastic behavior of the Earth's crust can be monitored through the analysis of the Earth's seismic response and its evolution with time. This kind of analysis is particularly interesting when combined with the reconstruction of seismic Green's functions from the cross-correlation of ambient seismic noise, which circumvents the limitations imposed by a dependence on the occurrence of seismic events. In fact, because seismic noise is recorded continuously and does not depend on earthquake sources, these cross-correlation functions can be considered analogously to records from continuously repeating doublet sources placed at each station, and can be used to extract observations of variations in seismic velocities. These variations, however, are typically very small: of the order of 0.1%. Such accuracy can be only achieved through the analysis of the full reconstructed waveforms, including later scattered arrivals. We focus on the method known as Moving-Window Cross-Spectral analysis that has the advantage of operating in the frequency domain, where the bandwidth of coherent signal in the correlation function can be clearly defined. We investigate the sensitivity of this method by applying it to microseismic noise cross-correlations which have been perturbed by small synthetic velocity variations and which have been randomly contaminated. We propose threshold signal to noise ratios above which these perturbations can be reliably observed. Such values

are a proxy for cross-correlation convergence, and so can be used as a guideline when determining the length of microseismic noise records that are required before they can be used for monitoring with the moving-window cross-spectral technique.

Key words: microseismic noise – cross-correlation – seismic monitoring.

1 INTRODUCTION

Stress field variations in time modify the elastic behavior of the Earth's crust, hence they can be recovered through the analysis of the Earth's seismic response and its temporal evolution. This is particularly true when earthquake codas, microtremors or microseismic noise are considered, as these are very sensitive to the effects of the often small perturbations in the Earth's elastic properties as they sample it both randomly and repeatedly (Aki 1957; Sato & Fehler 1998). Much effort has been devoted to the study of waveform variations in space and time for the purpose of understanding the dynamic behaviour of the crust. Of particular interest are tectonically and volcanically active regions in which stress changes are frequent and may precede earthquakes and volcanic eruptions. Initially, almost all studies focused on the spatio-temporal behavior of coda waves, where the observation of variations in their amplitude found a possible application in the forecasting of volcanic activity (Aki & Ferrazzini 2000). The inclusion of phase information to the analysis (Poupinet et al. 1984) gave rise to a new approach which led to the detection of relative variations in seismic velocity between earthquake doublets and multiplets. In the same way, the seismic coda wave interferometry technique developed by Snieder et al. (2002) has confirmed the existence of detectable precursory crustal changes (Grêt et al. 2005; Wegler et al. 2006), but is only practicable in cases where records of highly similar earthquake doublets are available.

More recently, seismic noise has become an increasingly popular and promising area of study, as it circumvents the limitations imposed by a dependence on the occurrence of seismic events. This is due to the possibility of retrieving seismic Green's functions from the cross-correlation of records of a random seismic wave field taken at various locations within a region of interest

(Weaver & Lobkis 2001; Lobkis & Weaver 2001; Campillo & Paul 2003; Shapiro & Campillo 2004; Shapiro et al. 2005; Sabra et al. 2005). Indeed, the use of ambient noise cross-correlations for monitoring has been shown to be robust even when conditions prevent the full reconstruction of the seismic Green's function (C. Hadziioannou et al. 2009; Weaver et al. 2009).

Because seismic noise is recorded continuously and does not depend on earthquake sources, these cross-correlation (cc) functions can be considered analogously to records from continuously repeating doublet sources placed at each station, and can be similarly used to extract observations of variations in seismic velocities.

The main idea for monitoring the evolution of seismic velocities over time using seismic noise is to compare "current" cross-correlation functions that represent the situation at a given time period to "reference" functions that represent an average background state of the studied media. We can distinguish between two different approaches that are used for the extraction of seismic velocity variations from cross-correlations and operate in the time and frequency domains, respectively. The first method, known as Coda Wave Interferometry, was described by Snieder (2006), and later evolved to Passive Image Interferometry (Sens-Schönfelder & Wegler 2006; Wegler et al. 2009) for noise sequence cross-correlations. The second method has been named Moving-Window Cross-Spectral Analysis (MWCS) by Ratdomopurbo & Poupinet (1995) and is the focus of the present study. In fact, although approaches in both the time and frequency domains have found interesting applications showing similar sensitivities (Wegler et al. 2009), the MWCS technique has the advantage of operating in the frequency domain, where the bandwidth of coherent signal in the correlation function can be clearly defined.

The main goal of this paper is to assess the accuracy of the velocity variations measured from noise cross-correlations with the MWCS technique and, in particular, how this accuracy depends on the quality (i.e., signal to noise ratio, SNR) of the reconstructed cc functions. We start by briefly introducing the main concepts of the MWCS method with most of the technical details described in Appendix A. Then, we use a set of noise cross-correlations computed from records of the seismic stations of the Piton de la Fournaise volcano (La Réunion) monitoring network shown in Figure 1.

First, we study the convergence of these cc functions and their fluctuations in the time and

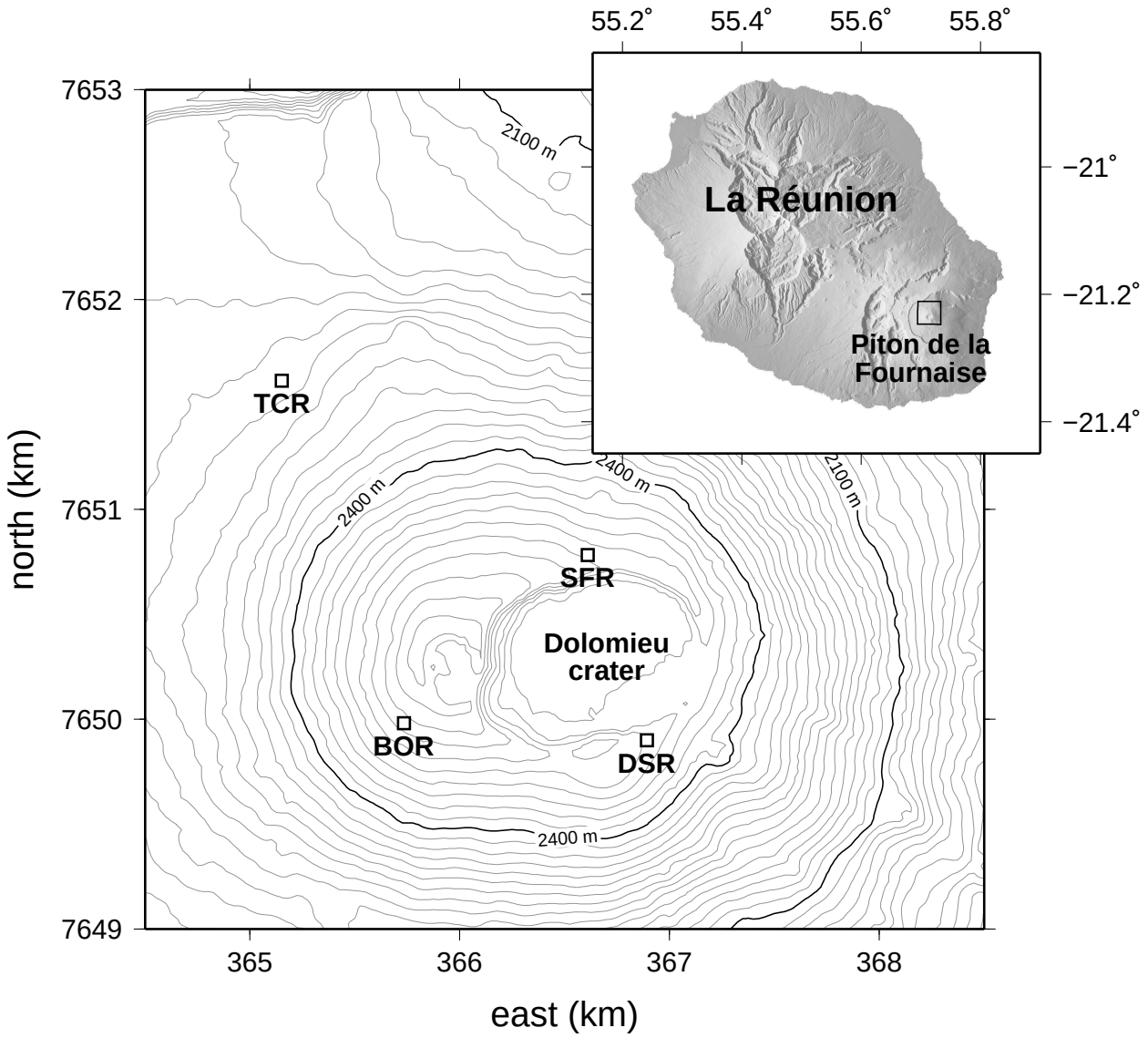

Figure 1. Map of stations (named black squares) used in this study. *inset:* La Réunion island. The black box outlines the part of Piton de la Fournaise shown in the main panel.

frequency domains. Then, we construct a set of synthetic reference and current cc functions by stretching the observed cc functions to mimic velocity variations within the media and by adding random noise with spectral properties similar to observed random variations. We apply the MWCS measure to these synthetic cc functions and compare the inferred velocity variations with known a-priori introduced values. We finally propose threshold values of SNR above which small velocity variations can be reliably retrieved and subsequently interpreted.

2 MOVING-WINDOW CROSS-SPECTRAL ANALYSIS

The Moving-Window Cross-Spectral technique was first introduced by Poupinet et al. (1984) for the retrieval of relative velocity variations between earthquake doublets. More recently, Brenguier et al. (2008a,b) exploited this technique by applying it to seismic noise records, taking advantage of the possibility of treating noise cross-correlations in analogy with doublets. Here we describe only the general purpose of the technique, leaving all computational details to Appendices A and C.

This analysis is applied to time series which are computed by cross-correlating the noise sequences recorded at two different seismic stations, for all possible station pairs. The preliminary step for the analysis is to build up at least one reference and several current cross-correlations. Since, for computational purposes, the continuous noise records are cut into short sequences (for example, one for each day or hour), it is necessary to stack a certain number of single cc's. In this framework, the reference and current functions are defined by the number of summed cc's: N_{ref} and N_{cur}, respectively. The only requirement is that $N_{ref} >> N_{cur}$ to ensure the reference cc is representative of a background value, while the current cc contains information on the actual state of the crust.

For any couple of reference, cc_{ref}, and current, cc_{cur}, functions, the technique combines two steps. The first step consists in the computation of the time-delay between the two signals within a series of overlapping windows. The second step is the evaluation of the relative velocity variation associated to the current function with respect to the reference. In this second step, it is assumed, for simplicity, that the seismic wave propagation velocity is perturbed homogeneously within the studied media.

It is important to note that the first operation is executed in the spectral domain, through the study of the phase of the cross-spectrum, allowing for precise selection of the frequency band on the basis of the coherency between the two windowed cc's (see Appendix A1). Each computed delay-time corresponds to a cross-correlation lag-time, which is taken as the central point of the window. Therefore, the second step involves the evaluation of the trend, $\delta t/t$, of the delay-time estimates over the whole length of the signals (see Figure A1). The slope of their linear regression

indicates, to a first approximation, the relative homogeneous velocity perturbation of the current cc with respect to the reference cc.

Critical points in the MWCS analysis are the choices of N_{ref}, N_{cur}, the length and overlap of each window and the total number of windows which are used. These are all required for the first step. The choice of these parameters will depend on the characteristics of the cc functions such as their length, frequency content and how fast the signal decays below the noise level. The aim of our work is to test the reliance of both the resolution and accuracy of the measurements on the quality of the cc functions, which can be quantified in terms of their signal to noise ratio.

3 RANDOM FLUCTUATIONS AND CONVERGENCE OF OBSERVED NOISE CROSS-CORRELATIONS

Measuring the signal to noise ratio (SNR) of a stacked set of cross-correlation functions is needed to distinguish between stacks from which reliable delay-times can be measured, and those from which they cannot. Furthermore, the simulated SNR of the cross-correlations we use in our tests must be compatible with this measure. We employ the method described by Larose et al. (2007), which is summarized below.

First, to estimate the level of noise, $\sigma(N,t)$, in a stack, we measure the variation between each constituent cross-correlation function, $cc(t)$, at each lag-time, t, as follows

$$\sigma(N,t) = \sqrt{\frac{\langle cc(t)^2\rangle - \langle cc(t)\rangle^2}{N-1}} \tag{1}$$

Here, $\langle\cdot\rangle$ denotes the average over N single functions. We then measure the level of signal, $s(N,t)$, in the stacked cross-correlation by taking its Hilbert envelope

$$s(N,t) = |\langle cc(t)\rangle + iH(\langle cc(t)\rangle)| \tag{2}$$

where $H(\cdot)$ denotes the Hilbert transform of the stacked function $\langle cc(t)\rangle$ and i is the imaginary unit. After we smooth $s(N,t)$ and $\sigma(N,t)$ with a ten-second-wide sliding cosine window, the SNR of the stacked cross-correlation function can be estimated

$$SNR(N,t) = \frac{s(N,t)}{\sigma(N,t)} \tag{3}$$

Figure 2 demonstrates the measurement of SNR using this method. The plotted cross-correlations are from stations DSR and TCR near the summit of Piton de la Fournaise volcano, La Réunion (Figure 1), during the thirty days preceding an eruption on its northern flank (Peltier 2007). Neither the variation between the daily functions nor the estimated signal are constant with t. The resulting signal to noise ratio, however, is less variable. For the purpose of our tests, we simulate a signal to noise ratio which is constant for all t when we add noise to our cross-correlation functions.

Figure 3 shows how the SNR of a cross-correlation stack depends on N. Here, we stack various numbers of consecutive daily cross-correlations from stations DSR and TCR. Days of missing data and of eruptive activity are skipped, and the plotted values of N are the number of remaining days. This plot shows that SNR grows at a rate which is just less than proportional to $\sqrt{N}$. While SNR appears to increase monotonically with N, it may in many instances be affected by drastic changes in the geology of the region under investigation. In this example, we avoid the collapse of Dolomieu crater at the start of 2007 on the summit of Piton de la Fournaise volcano by only using cross-correlations between the years 1999 and 2006.

Figure 4 shows the relationship between the error estimated by the MWCS technique (e_b defined by Equation A.12 in Appendix A2) and the SNR calculated above. Here, current- and reference functions are formed by grouping daily cross-correlations from stations DSR–TCR into 30-day and 300-day stacks, respectively. For each current and reference function pair between the years 1999 and 2006, we measure delay-times within 6 second-wide lag-time windows. We then attribute the mean current function SNR within each window to its corresponding delay-time δt. Finally, we calculate $\delta t/t$ along with its accompanying error as explained in Appendix A. This error, expressed relative to $\delta t/t$, is plotted against the mean of the attributed SNR values. For each of the plotted ranges of $|\delta t/t|$, these errors appear to be anti-correlated with SNR. Figure 5 summarizes these observations for station pairs DSR–TCR and BOR–SFR. These plots show a consistent inverse proportionality between the errors and the calculated SNR values, verifying that this measure of SNR may be eventually used to assess the quality of the $\delta t/t$ measurement obtained from noise correlations.

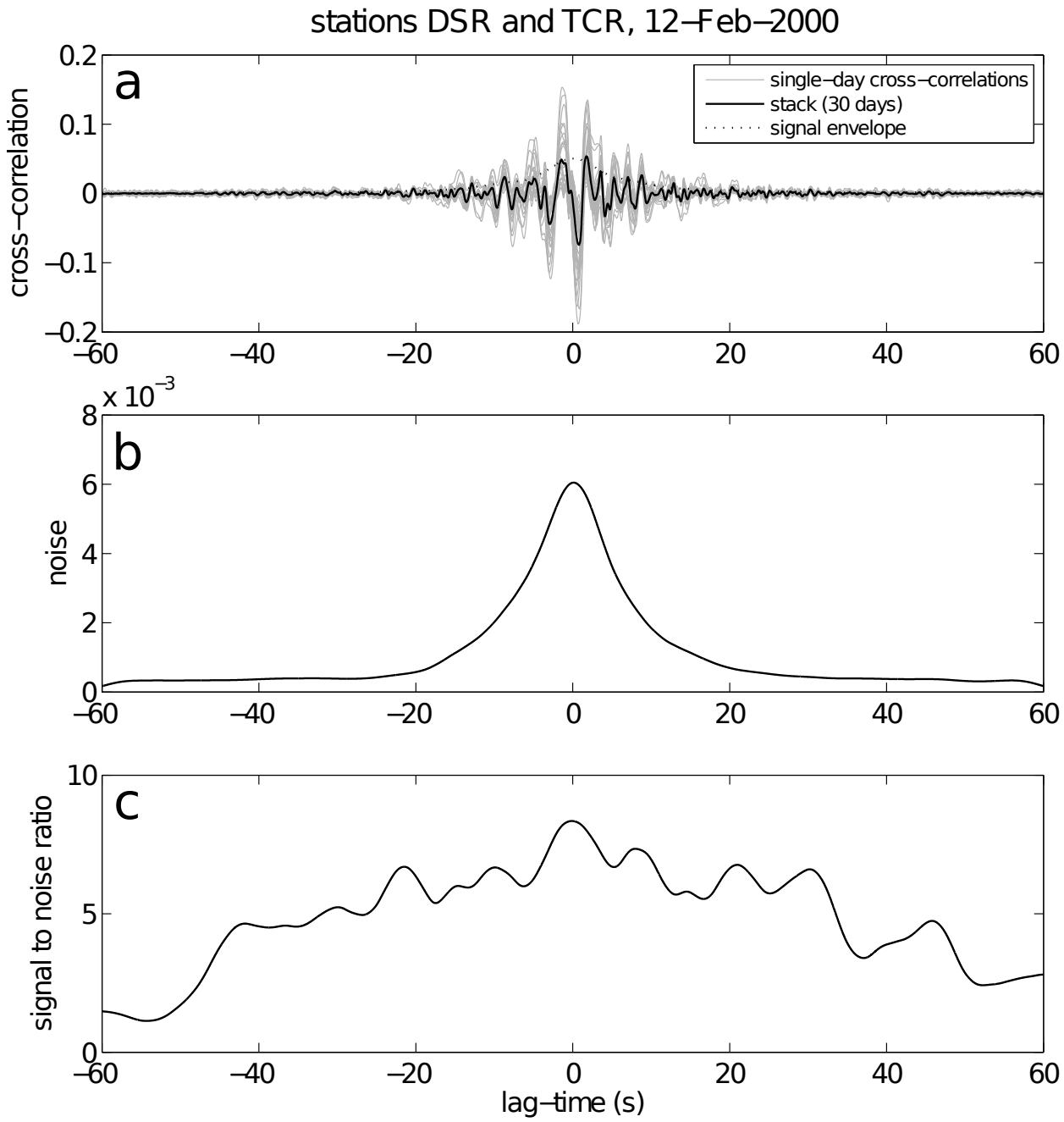

Figure 2. The calculation of SNR. *a:* A set of thirty single-day cross-correlation functions (grey curves) and their stacked mean (solid black curve). The dotted black curve is the signal envelope of the stack, and is smoothed with a ten-second-wide cosine window. *b:* The smoothed noise measured from this set of cross-correlations. *c:* The resulting SNR is the ratio of the signal envelope and the noise.

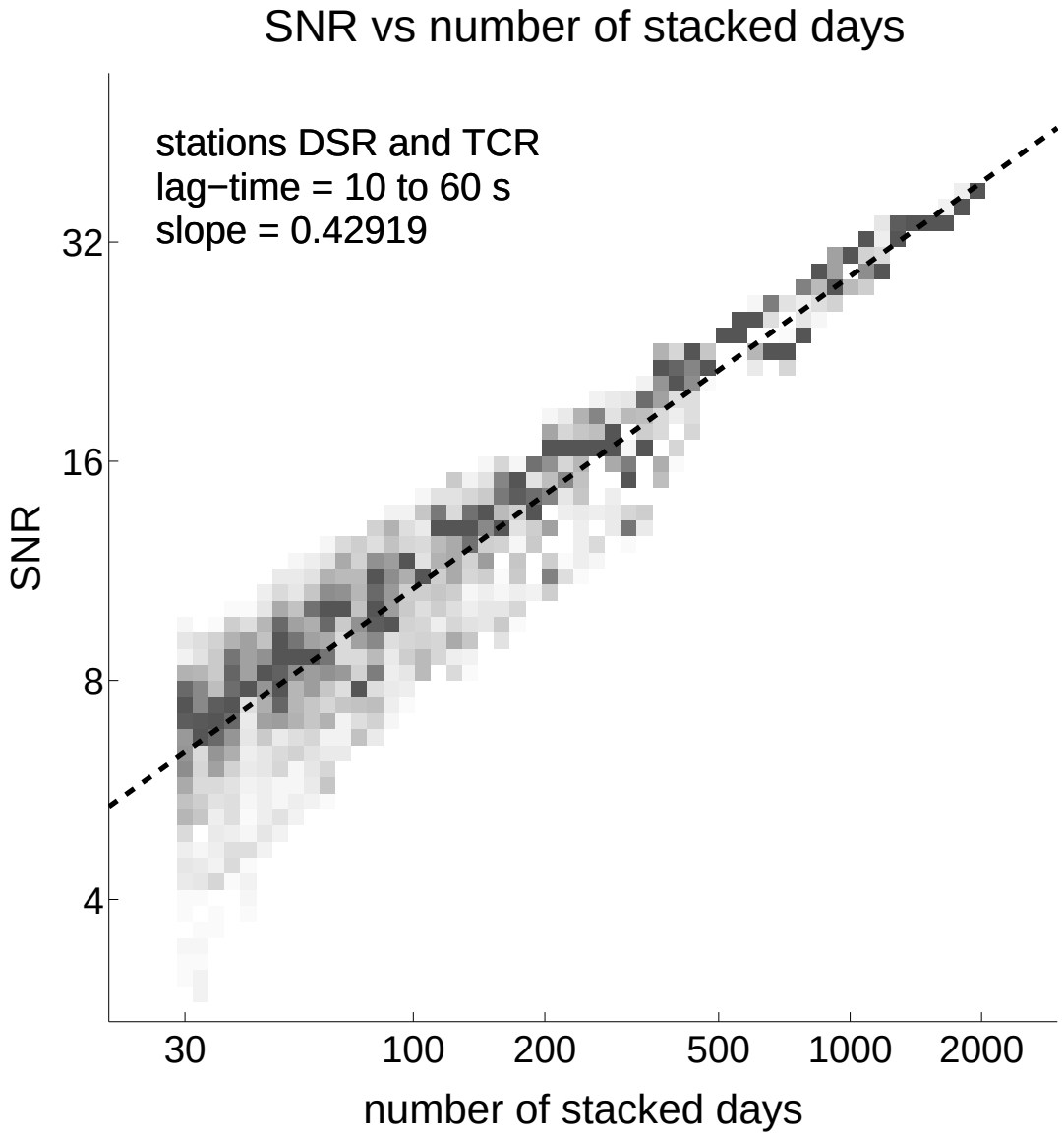

Figure 3. A plot of SNR versus number of stacked days (N). Results are separated into bins of $ln(N)$ and $ln(SNR)$. Counts are plotted as shades of grey after normalization within each column of the plotted grid. Dark shaded bins have high counts relative to lightly shaded bins. SNR is averaged over $|t| > 10$ seconds. The dashed curve and displayed slope are from a linear regression of the plotted values.

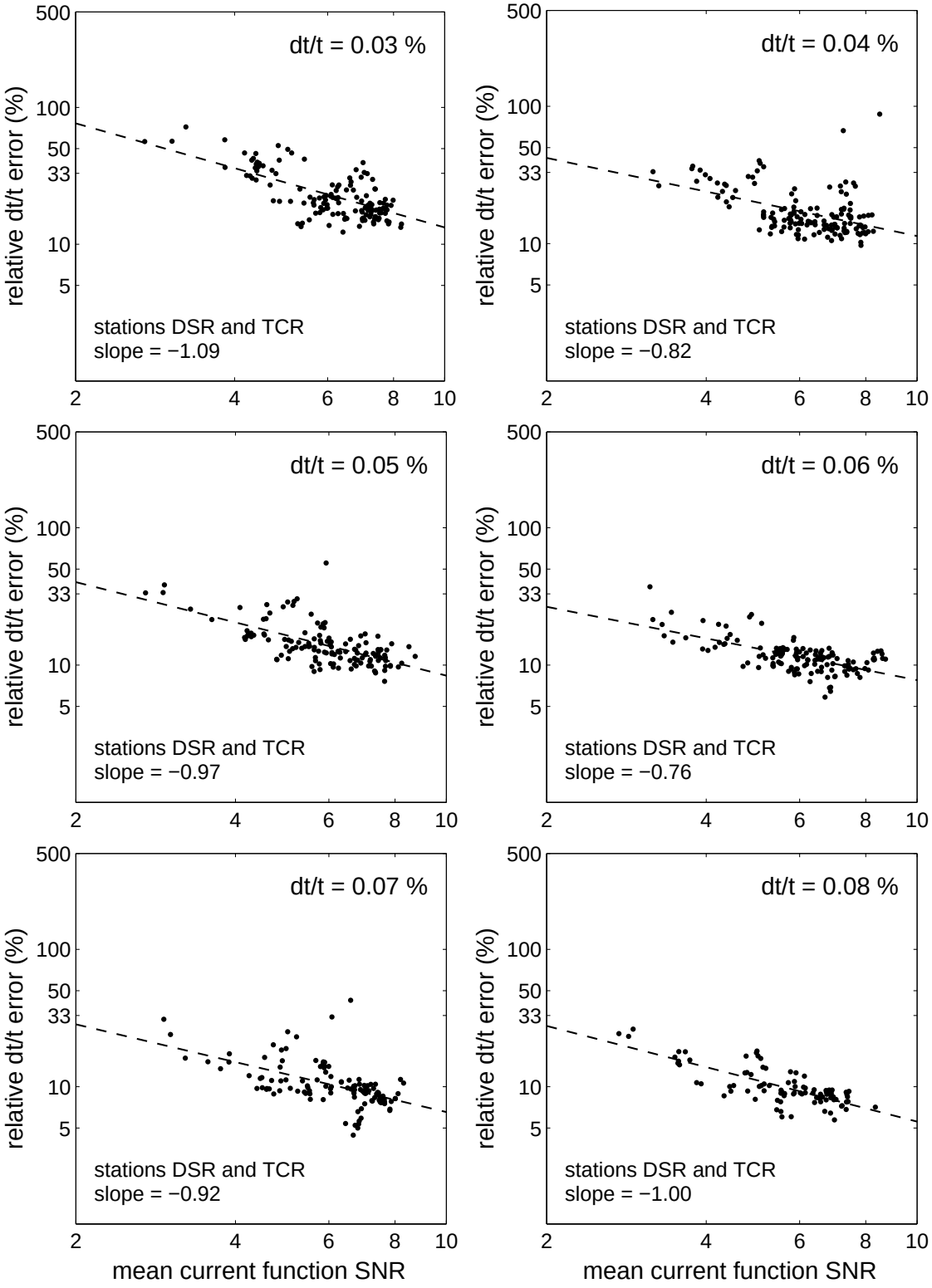

Figure 4. Relative $\delta t/t$ error estimates versus SNR for station pair DSR–TCR. Each panel pertains to a different range of $|\delta t/t|$. Dashed curves and displayed slopes are obtained via linear regressions of the plotted values.

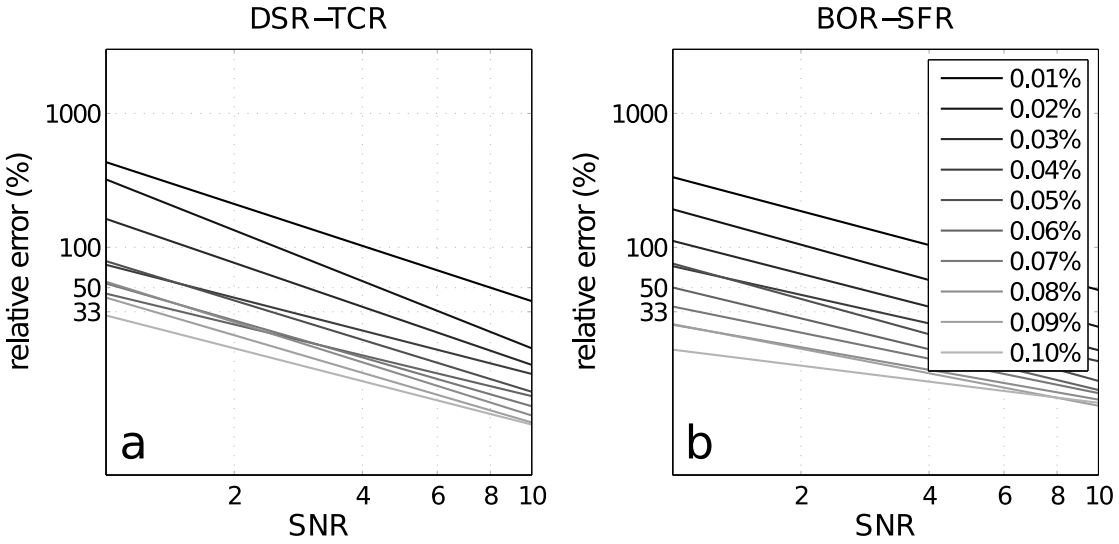

Figure 5. Lines of best fit determined from relative $\delta t/t$ error estimates for (*a*) stations DSR–TCR and (*b*) BOR–SFR. One line is plotted for each value of $|\delta t/t|$ (see legend).

4 SYNTHETIC CROSS-CORRELATION FUNCTIONS

To test the sensitivity of the MWCS technique, we construct a synthetic data set as follows: first, we take a reference function from real cross-correlations of seismic noise, then stretch it to simulate a series of homogeneous seismic velocity changes. This stretch is achieved by resampling the cross-correlations with a Fourier-transform based interpolation. Effectively, this involves zero-padding the cross-correlation in the Fourier-domain, then taking the inverse transform. When the original sampling interval is applied, the interpolated cross-correlation becomes a stretched version of the original. We then add random noise to each stretched cross-correlation function to simulate a set of possible signal to noise ratios. Finally, treating the original function as the reference, and each stretched, noise-added function as the current function, we attempt to recover the applied stretch using the MWCS method and to see how the resulting errors depend on the level of the added noise. For these tests it is important to use synthetic noise with properties close to the real random fluctuations of the observed cc functions. Therefore, we first characterize the spectra of these observed fluctuations and then propose a procedure to simulate a random noise series with defined spectral properties.

4.1 Spectrum of the observed random fluctuations

A simple way to view a pair of stacked current and reference cross-correlation functions is to treat the current function, $cc_{cur}(t)$, as a contaminated version of the relatively noiseless reference function, $cc_{ref}(t)$.

$$cc_{cur}(t) = cc_{ref}(t) + n(t) \tag{4}$$

To observe one realization of the impinging noise, $n(t)$, we simply subtract the current function from the reference function.

Figure 6 shows an example of a current and a reference function computed for stations DSR and TCR on Piton de la Fournaise volcano, La Réunion. The reference function is a stack of the 300 days preceding an eruption on the volcano's south-eastern flank (Peltier 2007), while the current function is a stack of the last thirty of those days. Although the level of the noise appears

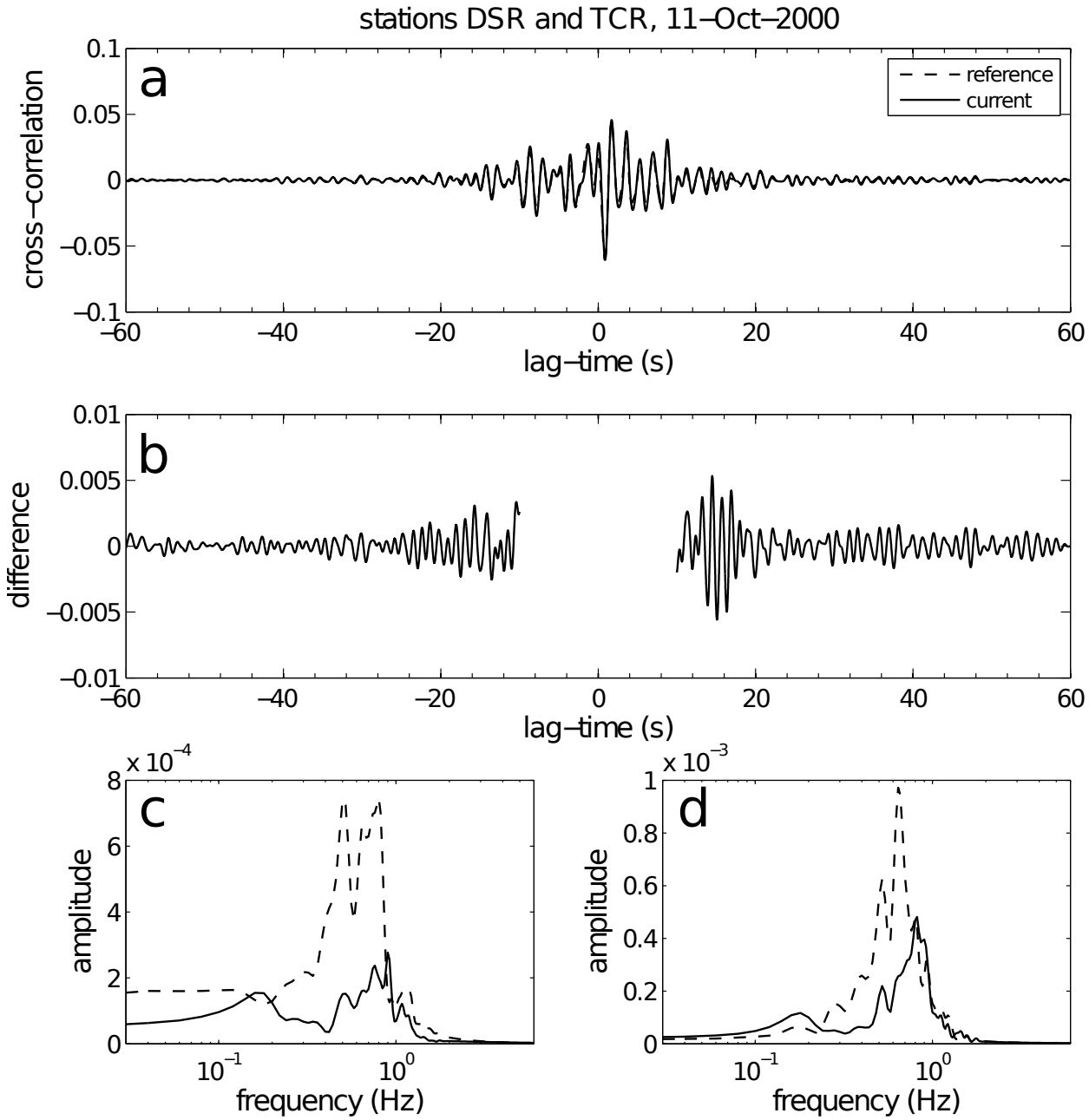

Figure 6. Observation of noise in real cross-correlation stacks. *a:* A 300-day reference stack (dashed curve) and its associated 30-day current stack (solid curve). *b:* The difference between the reference and current stack is taken as an observation of noise. Small lag-times are omitted from the calculation as they are not used for delay-time estimation. *c* and *d:* Amplitude spectra of the negative-lag and positive-lag segments, respectively, of the observed noise (solid curves) and the reference stack (dashed curves).

to be relatively low compared to that of the reference function, examination of its spectrum reveals that the amplitude of the noise is at least comparable to that of the reference function at certain frequencies.

For every station pair, we calculate $n(t)$ for all available current and reference function pairs between the years 1999 and 2006. Then, by averaging their squared-amplitude spectra, we ob-

serve a typical noise spectrum which we can use to contaminate our synthetically stretched cross-correlation functions (e.g., Figure 6c and 6d).

4.2 Simulating random noise with pre-defined spectra

To contaminate our synthetic cross-correlation functions, we randomly perturb each value by an amount drawn from a Gaussian distribution. The standard deviation of this distribution is chosen as follows

$$\sigma_{synth}(t) = \frac{s(t)}{SNR(t)} \tag{5}$$

where $s(t)$ is the signal envelope of the synthetic function, and $SNR(t)$ is the desired signal to noise ratio. We discuss whether or not the use of a Gaussian distribution to simulate noise in this way is appropriate for our cross-correlations in Appendix D.

To ensure that the noise exists in the appropriate frequency band, we apply the method described by Percival (1993) to produce a random time-series which shares the same spectrum as that observed in real data. After normalizing to unit standard deviation, we scale the resulting noise by $\sigma_{synth}(t)$, then add it to our synthetic cross-correlation function.

Figure 7 demonstrates how noise is prepared in this way. The original function is a stack of all available daily cross-correlations computed between stations DSR and TCR in the year 2002. Noise is generated using the spectrum which is observed for this station pair, then scaled to produce a constant signal to noise ratio. This noise targets the frequency range in which real noise is observed and in which delay-times are to be later measured.

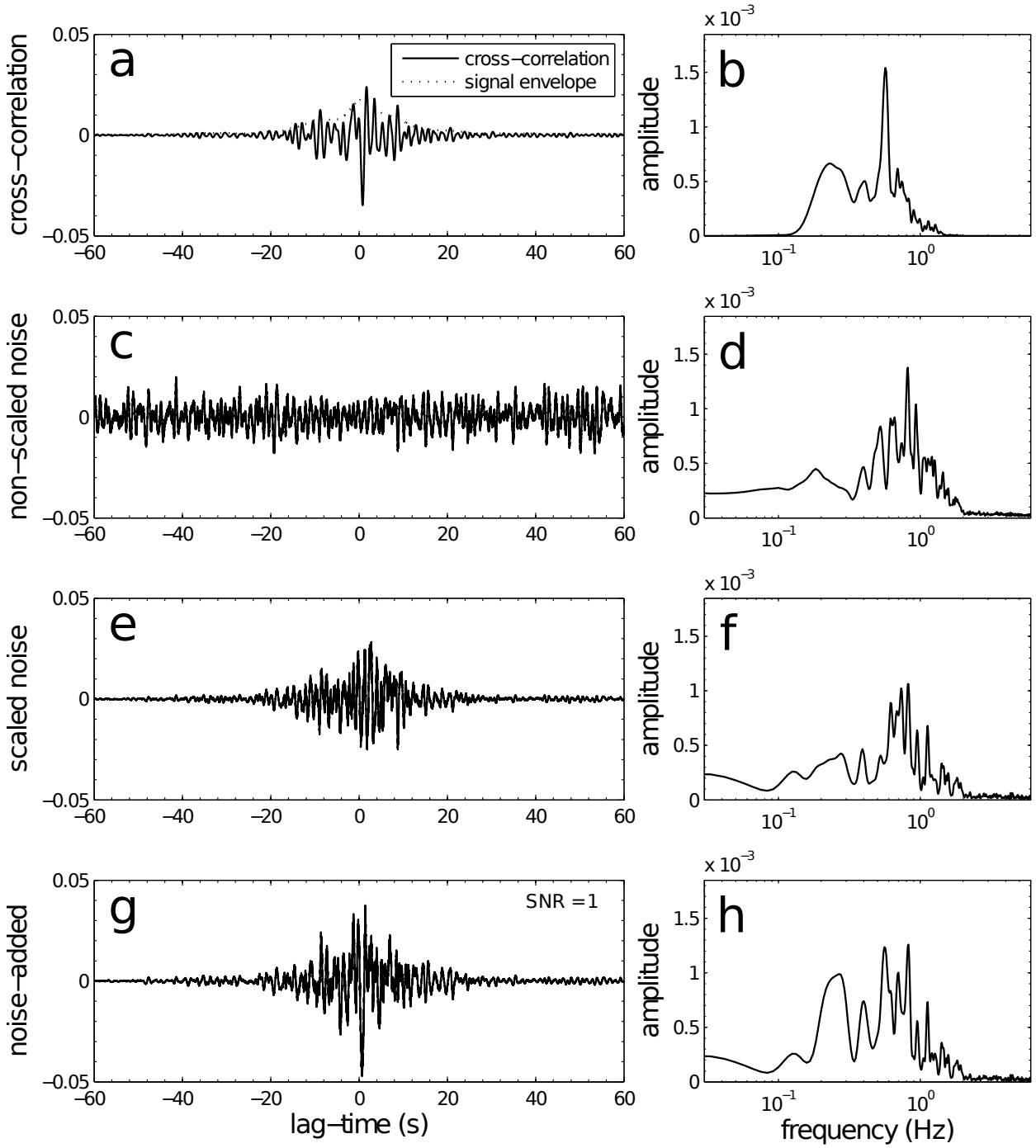

Figure 7. Addition of random noise to a synthetic cross-correlation function from stations DSR and TCR. The signal level (*a*, dotted curve) is estimated from the original function (solid curve). Panel *b* shows the spectrum of the cross-correlation function. Random Gaussian noise (*c*) is produced with a spectrum (*d*) that simulates that of the noise which is observed for the station pair. This noise is scaled in time (*e* and *f*), then added to the original cross-correlation function (*g* and *h*).

5 RESULTS OF SYNTHETIC TESTS

For every station pair, we simulate 1000 random synthetic realizations of current cc functions with predefined stretching coefficients mimicking velocity perturbations and predefined signal to noise ratios. Then, we analyze the resulting set of $\delta t/t$ (stretch) estimates and their accompanying errors.

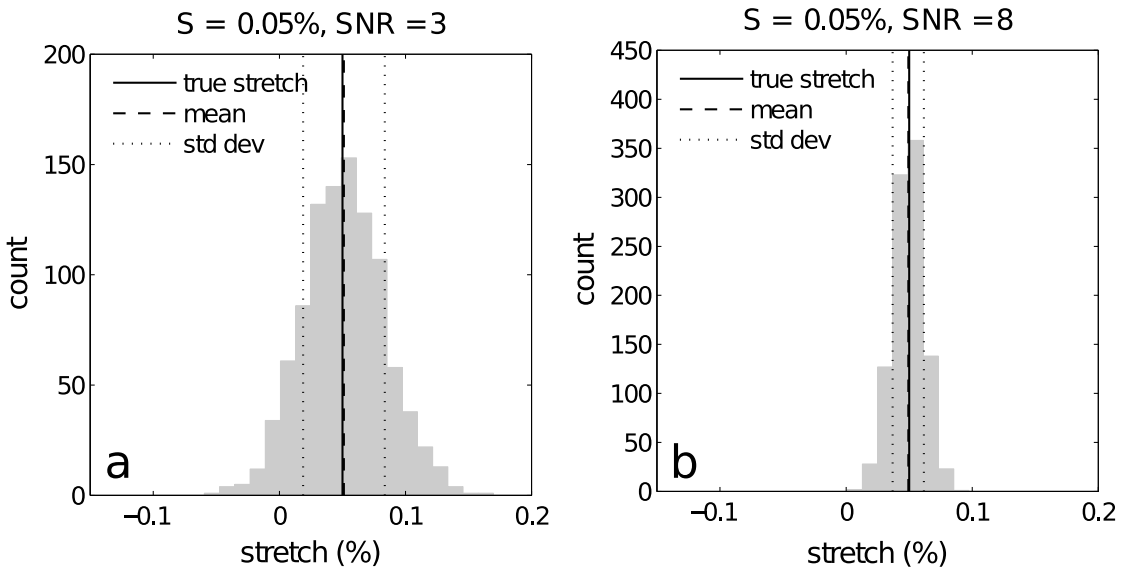

Figure 8. Histograms for two sets of stretch estimates. *a:* The applied stretch is 0.05 % and the simulated SNR is 3. *b:* The applied stretch is unchanged, but the simulated SNR is increased to 8. The reference cross-correlation is from stations DSR and TCR.

We show results of sensitivity tests for vertical-component records from two pairs of stations on Piton de la Fournaise volcano, La Réunion. For each station pair (BOR–SFR, and DSR–TCR), we stack every available daily cross-correlation function between the years 1999 and 2006 to construct our reference function, then filter between 0.1 and 1.0 Hz.

To construct current functions, we stretch these reference cross-correlations by a range of values, $S = \{0.01\%,\ 0.02\%, \ldots ,\ 0.10\%\}$, then add noise to simulate signal to noise ratios of $SNR = \{1,\ 2, \ldots ,\ 10\}$. Finally, we use six-second-wide lag-time windows which overlap by three seconds to compute delay-times (See Appendix A).

For each pair of simulated stretch and SNR values (S, SNR), we obtain 1000 stretch estimates, S_i, $i \in [1, 1000]$, and their associated least-squares errors, e_i (standard deviations) from the MWCS technique. Figure 8 shows the distribution of these estimates for two different values of SNR. In both cases, these estimates form an approximately bell-shaped distribution centered around the true stretch of 0.05%. In the case of low SNR, these estimates form a wide distribution (Figure 8a) due to the high level of noise in the cross-correlations, and we cannot confidently recover $\delta t/t$. When SNR is increased (Figure 8b), the distribution narrows, and $\delta t/t$ is better resolved.

To quantitatively assess the level of systematic error in each set of estimates, we calculate their relative bias as follows

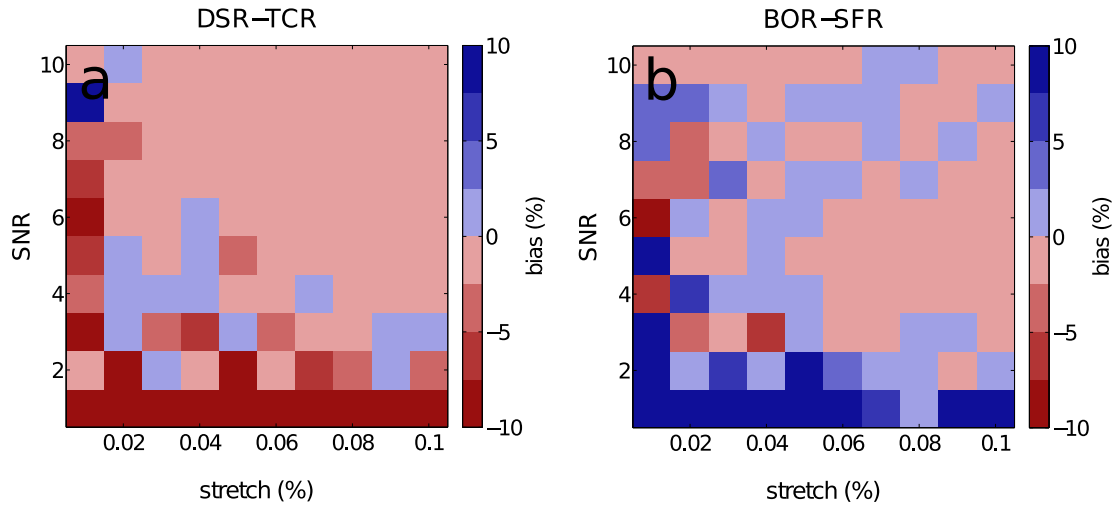

Figure 9. Relative bias calculated for each (S, SNR) pair using Equation 6. Cross-correlation functions are taken from (*a*) stations DSR–TCR and (*b*) stations BOR–SFR. Light colours indicate a small relative bias.

$$b(S, SNR) = \frac{\langle S_i \rangle - S}{S} \tag{6}$$

Figure 9 shows this measure for stations DSR–TCR (Figure 9a) and BOR–SFR (Figure 9b). For both station pairs, the relative bias is never more than a few percent, provided the simulated stretch and SNR are large enough (say, above 0.02% and 3, respectively). This suggests the MWCS method introduces very little systematic error.

To assess the total relative error over the 1000 trials for each (S, SNR) pair, we calculate their misfit from the true stretch as follows

$$e_{total}(S, SNR) = \frac{1}{S} \times \sqrt{\frac{\sum (S_i - S)^2}{1000 - 1}} \tag{7}$$

This incorporates both the systematic and the random error in each set of 1000 S_i estimates. Figure 10 shows these measures for the two station pairs described above. Here, colors indicate the level of error, expressed as a percentage of the true stretch. As expected, this error decreases as either the applied stretch or the simulated SNR are increased.

We compare this error, e_{total}, evaluated from the synthetic test with errors evaluated from the least-squares fit during the MWCS analysis (Appendix A2). For every synthetic current cc function, we evaluate the least-squares error and then compute its mean value for a given pair of stretching coefficient and SNR $\langle e_i \rangle (S, SNR)$. Figure 11 shows the ratio of errors estimated from

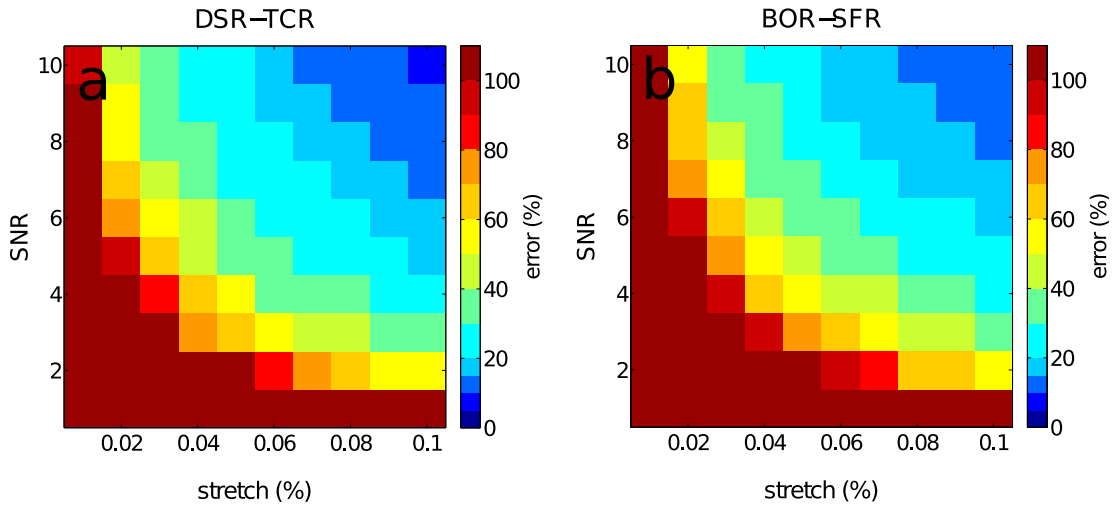

Figure 10. Total errors calculated for each pair using equation 7. Cross-correlation functions are taken from (*a*) stations DSR–TCR and (*b*) stations BOR–SFR. Cold colours indicate (S, SNR) values for which $\delta t/t$ is well resolved using the MWCS technique.

the synthetic test and from the MWCS least-squares fit for station pairs DSR–TCR and BOR–SFR. For both station pairs, the least-squares error underestimates the total variability of the targeted velocity variations by a factor of around six for most values of SNR and for all applied stretching coefficients (Figure 11). We address the cause of this discrepancy in Appendix B.

Finally, we plot e_{total} against SNR (Figure 12) to see if the estimates we obtain during our tests exhibit the inverse relationship between cross-correlation quality and $\delta t/t$ error that we see for real

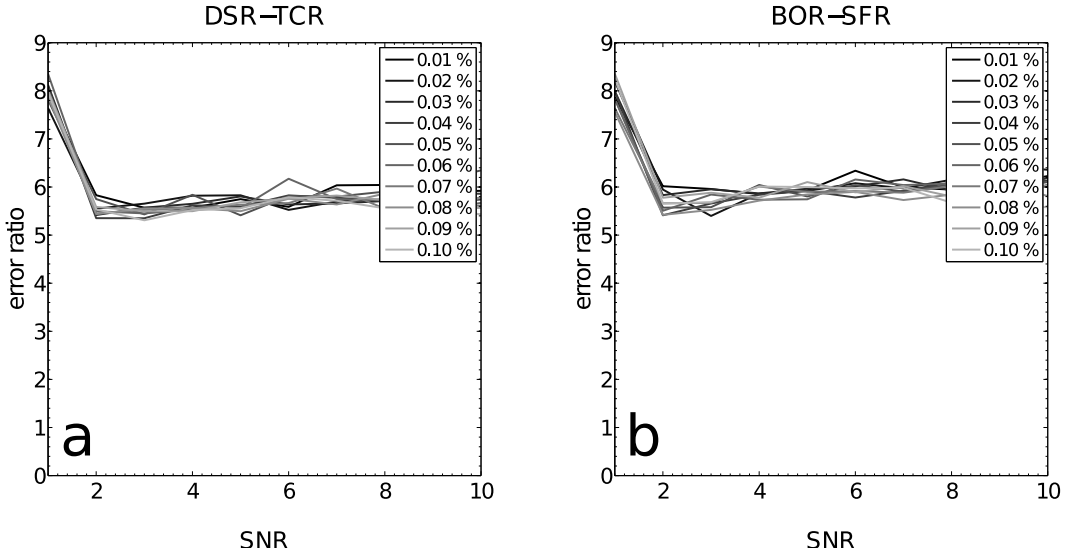

Figure 11. Ratio between the total error and the error estimated from the MWCS least-squares fit as a function of SNR. Cross-correlation functions are taken from (*a*) stations DSR–TCR and (*b*) stations BOR–SFR. One line is plotted for each simulated stretch (see legend).

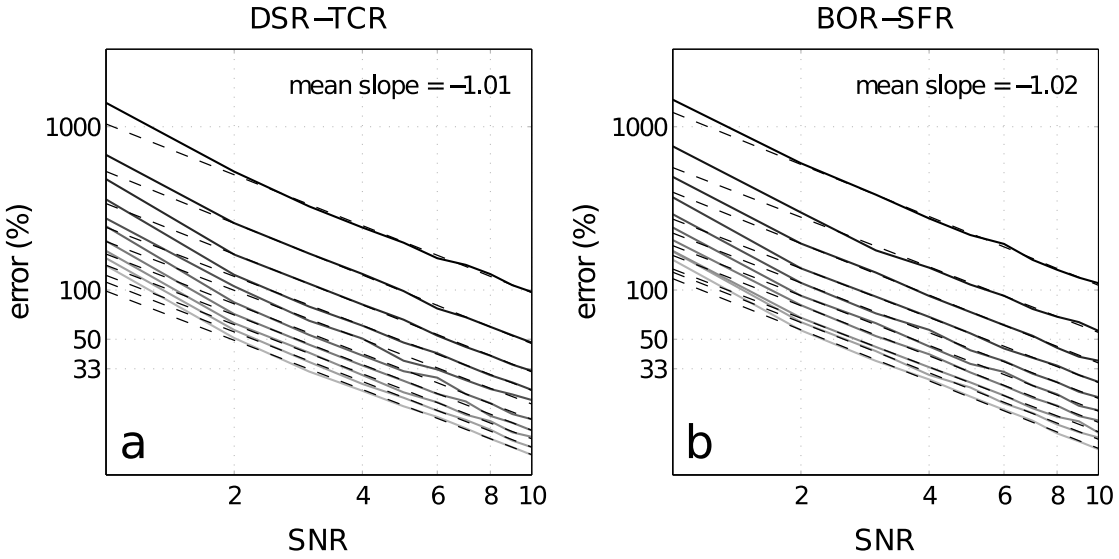

Figure 12. Total error plotted as a function of SNR. Cross-correlation functions are taken from (*a*) stations DSR–TCR and (*b*) stations BOR–SFR. One line is plotted for each simulated stretch (see legend in Figure 11) along with its estimated slope (dashed lines).

data (Figures 4 and 5). When viewed on a log-log scale, these results exhibit a clear anticorrelation. Reassuringly, the similarity between this plot and Figures 4 and 5 demonstrates the consistency between the SNR we simulate and the SNR we measure from real data.

6 DISCUSSION AND CONCLUSIONS

To assess the accuracy of the velocity variations measured from noise cross-correlations (CC) with the MWCS technique we constructed a set of synthetic CC functions corresponding to known media velocity variations (stretching coefficients) and perturbed by random noise with statistical properties similar to those observed at the stations of the Piton de la Fournaise seismic network. Our analysis resulted in simple relations between the accuracy of the recovered velocity variations and the Signal-to-Noise Ratio (SNR) of the analyzed CC functions (Figure 10). In turn the SNR is on average simply related to the duration of the noise record from which the CC function was computed (Figure 3). These results provide us with a simple guidance on how to choose an optimal stack duration to recover a desired level of media velocity variations. In particular, for the case of the seismic stations on Piton de Fournaise volcano, our analysis indicated that recovering a relative velocity perturbation of 0.1% from a single pair of stations requires an SNR of ~ 5 that can be obtained by stacking a few tens of days of noise correlations. This implies in particular that the

accuracy of measurements presented by Brenguier et al. (2008b) by averaging measurements from many station pairs could be barely achieved from analyzing a single pair of stations.

Another important result of our analysis performed with synthetic CC functions is that the formal error computed from the linear regression within the MWCS technique does not match the true uncertainty of the recovered relative delay-times. In the case of our tests, the true error appears to be around six times greater than that which is estimated. This mismatch is mainly due to the fact that the least-squares error is not uniquely defined, but depends on the parameters used in the the application of the MWCS technique (See Appendix B). For a particular choice of parameters, this error may underestimate the real uncertainty of the recovered velocity variations. A further explanation is that the MWCS technique effectively uses only one realization of the CC function with a relatively short duration (because of the fast decay of the coda part of the recovered Green's functions). This single and short realization is not representative of the full variability of the CC functions. The sampling can be improved by using multiple pairs of stations simultaneously as has been done by Brenguier et al. (2008a,b). Nonetheless, the factor relating the MWCS error with the total error is roughly independent of both SNR and the media velocity variation. Furthermore, we observe the same factor (Figure 11) for both pairs of stations considered in our study, BOR–SFR and DSR–TCR. This means that, in the case of Piton de la Fournaise seismic noise cross-correlations, and for this particular choice of parameters, we can apply a correction to the MWCS errors by simply multiplying their values by a factor of ~ 6.

A main conclusion from our study is that before systematically applying noise-based MWCS monitoring of temporal media changes in a particular setting, it is important to investigate the statistical properties of the seismic noise and the convergence of noise correlations. This analysis is necessary to establish the correction factor for the MWCS errors and also the optimal durations of correlated time series. So far, our results indicate that recovering relatively weak velocity changes associated with moderate volcanic activity (Brenguier et al. 2008b), intermediate-size earthquakes (Brenguier et al. 2008a) or with seasonal variations (Meier et al. 2010) requires stacking correlations from a few tens of days and averaging measurements from many pairs of stations. Further improvement of temporal and spatial resolution of the MWCS measurements could be eventually

achieved by applying additional steps in the data processing such as data adaptive filtering (Baig et al. 2010).

ACKNOWLEDGMENTS

The seismogram data used in this study were provided by the Observatoire Volcanologique du Piton de la Fournaise. We thank Michel Campillo, Berenice Froment and Celine Hadziioannou for helpful discussions and G. Moguilny for maintaining the Cohersis cluster on which all computations were performed . This work was supported by Agence Nationale de la Recherche (France) under contracts ANR-06-CEXC-005 (COHERSIS) and ANR-08-RISK-011 (UNDERVOLC) and by a FP7 ERC Advanced grant 227507 (WHISPER).

REFERENCES

Aki, K., 1957. Space and time spectra of stationary stochastic waves, with special reference to microtremors, *Bull Earthquake Res Inst*, **35**, 415–456.

Aki, K. & Ferrazzini, V., 2000. Seismic monitoring and modeling of an active volcano for prediction, *J Geophys Res*, **105**, 16617–16640.

Baig A. M., Campillo, M., & Brenguier, F., 2010. Denoising seismic noise cross correlations, *J Geophys Res*, **114**, B08310, doi:10.1029/2008JB006085.

Brenguier, F., Campillo, M., Hadziioannou, C., Shapiro, N. M., Nadeau, R. M., & Larose, E., 2008a. Postseismic Relaxation Along the San Andreas Fault at Parkfield from Continuous Seismological Observations, *Science*, **321**(5895), 1478.

Brenguier, F., Shapiro, N., Campillo, M., Ferrazzini, V., Duputel, Z., Coutant, O., & Nercessian, A., 2008b. Towards forecasting volcanic eruptions using seismic noise, *Nature Geoscience*, **1**(2), 126.

Campillo, M. & Paul, A., 2003. Long-Range Correlations in the Diffuse Seismic Coda, *Science*, **299**(5606), 547–549.

Grêt, A., Snieder, R., Aster, R., & Kyle, P., 2005. Monitoring rapid temporal change in a volcano with coda wave interferometry, *Geophys Res Lett*, **32**(L06304).

Hadziioannou, C., Larose, E., Coutant, O., Roux, P., & Campillo, M., 2009. Stability of monitoring weak changes in multiply scattering media with ambient noise correlation: laboratory experiments, *J Acoust Soc Am*, **125**(6), 3688–3695.

Larose, E., Roux, P., & Campillo, M., 2007. Reconstruction of Rayleigh–Lamb dispersion spectrum based on noise obtained from an air-jet forcing, *J Acoust Soc Am*, **122**, 3437.

Lobkis, O. & Weaver, R., 2001. On the emergence of the Green's function in the correlations of a diffuse field, *J Acoust Soc Am*, **110**, 311–317.

Meier, U., Shapiro, N. M., & Brenguier, F., 2010. Detecting seasonal variations in seismic velocities within Los Angeles basin from correlations of ambient seismic noise, *Geophys J Int*, **181**, 985996, doi: 10.1111/j.1365-246X.2010.04550.x.

Peltier, A., 2007. *Suivi, modélisation et évolution des processus d'injections magmatiques au Piton de La Fournaise (Réunion), à partir d'une analyse croisée des données de déformation, géochimiques et structurales*, PhD these, Université de La Réunion.

Percival, D., 1993. Simulating Gaussian random processes with specified spectra, *Computing Science and Statistics*, pp. 534–534.

Poupinet, G., Ellsworth, W., & Frechet, J., 1984. Monitoring velocity variations in the crust using earthquake doublets: an application to the Calaveras faults, California, *J Geophys Res*, **89**, 5719–5731.

Ratdomopurbo, A. & Poupinet, G., 1995. Monitoring a temporal change of seismic velocity in a volcano: application to the 1992 eruption of Mt. Merapi (Indonesia), *Geophys Res Lett*, **22**(7), 775–778.

Sabra, K., Gerstoft, P., Roux, P., Kuperman, W., & Fehler, M., 2005. Extracting time-domain Green's function estimates from ambient seismic noise, *Geophys Res Lett*, **32**, L03310.

Sato, H. & Fehler, M., 1998. *Seismic wave propagation and scattering in the heterogeneous Earth*, Springer-Verlag.

Sens-Schönfelder, C. & Wegler, U., 2006. Passive image interferometry and seasonal variations of seismic velocities at Merapi volcano, (Indonesia), *Geophys Res Lett*, **33**(L21302).

Shapiro, N. M. & Campillo, M., 2004. Emergence of broadband Rayleigh waves from correlations of the ambient seismic noise, *Geophys Res Lett*, **31**(7).

Shapiro, N. M., Campillo, M., Stehly, L., & Ritzwoller, M. H., 2005. High-Resolution Surface-Wave Tomography from Ambient Seismic Noise, *Science*, **307**(5715), 1615–1618.

Snieder, R., 2006. The theory of coda wave interferometry, *Pure App Geophys*, **163**(2), 455–473.

Snieder, R., Grët, A., H., D., & J., S., 2002. Coda wave interfermotry for estimating nonlinear behavior in seismic velocity, *Science*, **295**, 2253–2255.

Stehly, L., Campillo, M., & Shapiro, N., 2007. Traveltime measurements from noise correlation: stability and detection of instrumental time-shifts, *Geophys J Int*, **171**, 223–230.

Weaver, R. & Lobkis, O., 2001. Ultrasonics without a Source: Thermal Fluctuation Correlations at MHz Frequencies, *Phys Rev Lett*, **87**(134301), 1–4.

Weaver, R., Froment, B., & Campillo, M., 2009. On the correlation of non-isotropically distributed ballistic scalar diffuse waves, *J Acoust Soc Am*, **126**(4), 1817-1826.

Wegler, U., Lühr, B.-G., Snieder, R., & Ratdomopurbo, A., 2006. Increase of shear wave velocity before the 1998 eruption of Merapi volcano (Indonesia), *Geophys Res Lett*, **33**(L09303).

Wegler, U., Nakahara, H., Sens-Schönfelder, C., Korn, M., & Shiomi, K., 2009. Sudden drop of seismic velocity after the 2004 M_w 6.6 mid-Niigata earthquake, Japan, observed with Passive Image Interferometry, *J Geophys Res*, **114**(B06305), 1–11.

APPENDIX A: MWCS

In the following section, the method of Moving-Window Cross-Spectral analysis (MWCS) is described in the context of stacked reference and current cross-correlation functions.

A1 Time-delay computation

The first step in the MWCS analysis is the calculation of delay-times, δt, between the two cross-correlation functions within a series of overlapping lag-time windows.

Each cross-correlation function is divided into N_w windows, one for each delay-time measurement. The choice of window length, overlap, and N_w will generally depend on the frequency content and the SNR of the cross-correlation functions under consideration. The windowed segments are mean-adjusted and cosine-tapered before being Fourier-transformed into the spectral domain.

In Figure A1 (a), an example of a windowed pair of cross-correlation functions is shown. The cross-spectrum, $X(\nu)$, between the two windowed time-series is calculated as follows

$$X(\nu) = F_{ref}(\nu) \cdot F^*_{cur}(\nu) \tag{A.1}$$

where $F_{ref}(\nu)$ and $F_{cur}(\nu)$ are Fourier-transformed representations of the windowed time-series, ν is frequency in Hz and the asterisk denotes complex conjugation. For our purposes, it is more useful to represent the complex cross-spectrum by its amplitude $|X(\nu)|$ and phase $\phi(\nu)$

$$X(\nu) = |X(\nu)|\, e^{i\phi(\nu)} \tag{A.2}$$

One requirement of cross-spectral time-delay estimation is that, aside from being shifted in time, the two windowed time-series are similar. Such similarity is quantitatively assessed using the cross-coherence $C(\nu)$ between their energy densities:

$$C(\nu) = \frac{\left|\overline{X(\nu)}\right|}{\sqrt{\overline{|F_{ref}(\nu)|^2} \cdot \overline{|F_{cur}(\nu)|^2}}} \tag{A.3}$$

Here, the overlines indicate smoothing, which in our case is obtained by applying a sliding raised-cosine function with a half-width of 0.1 Hz to the energy density spectra of the two Fourier-transformed time-series and to the real and imaginary parts of the complex-valued cross-spectrum. The cross-coherence ranges between zero and one, with maximum values approached at those frequencies where the two spectral densities are highly similar.

The time-delay between the two cross-correlations can be found in the (unwrapped) phase, $\phi(\nu)$, of the cross-spectrum, which will be linearly proportional to frequency.

$$\phi_j = m \cdot \nu_j, \qquad m = 2\pi\delta t \tag{A.4}$$

The time shift, δt_i (subscript i for the i^{th} window), between the two signals is estimated from the slope m of a linear regression of the samples, $j = l, ..., h$, within the frequency range of interest (see Figure A2, panel *c*). During the regression, a weight w_j, which depends on the cross-coherence at each sampled frequency, is assigned to each cross-phase value.

$$w_j = \sqrt{\frac{C_j^2}{1 - C_j^2} \cdot \sqrt{|X_j|}} \tag{A.5}$$

Unlike Poupinet et al. (1984), these weights incorporate both the cross-spectral amplitude and the cross-coherence. This generates more differentiated weights in cases where the cross-coherence is relatively constant but the cross-spectral energy is variable. Figure A2, panel *b* shows such an example. This choice of weighting is described in more detail in Appendix C.

Using a weighted least-squares inversion, the slope m is estimated as

$$m = \frac{\sum_{j=l}^{h} w_j \nu_j \phi_j}{\sum_{j=l}^{h} w_j \nu_j^2} \tag{A.6}$$

The associated error, e_m, is calculated using the rule of propagation of errors

$$e_m = \sqrt{\sum_j \left(\frac{w_j \nu_j}{\sum_i w_i \nu_i^2} \right)^2 \sigma_\phi^2} \tag{A.7}$$

where σ_ϕ^2 is the squared misfit of the data to the modeled slope and is calculated as

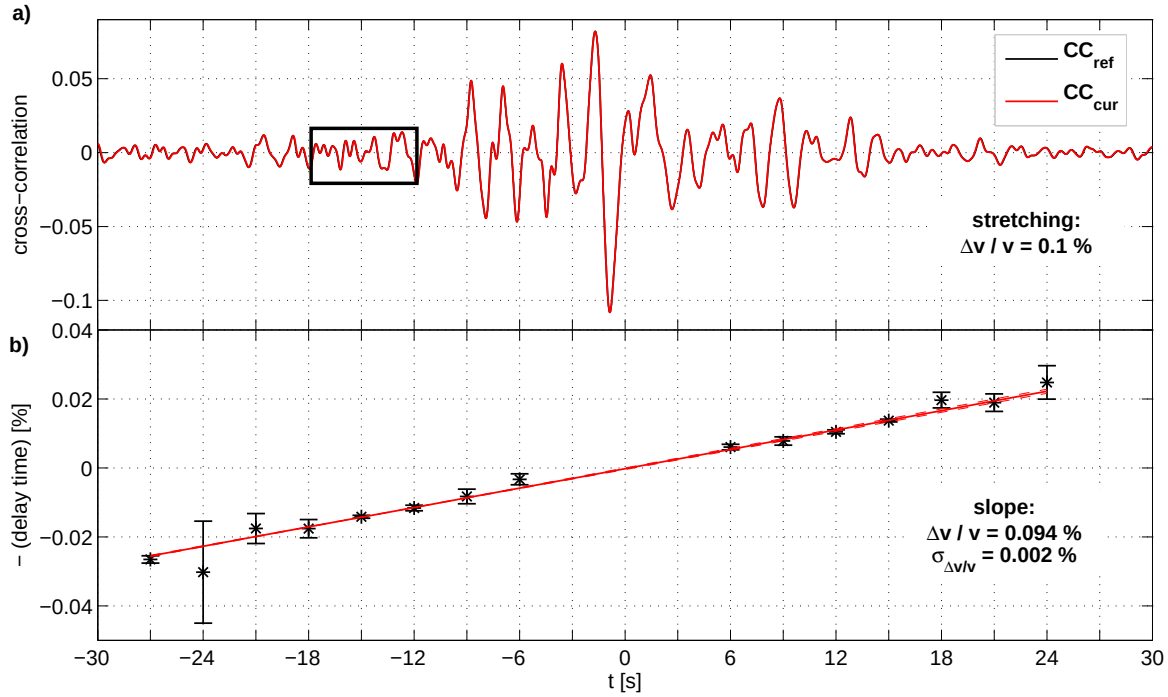

Figure A1. *a:* A pair of a real reference (from Piton de la Fournaise) and a synthetic current cross-correlation, along the time interval between -30 and 30 s. The current function is generated by stretching the reference by 0.1%. The black rectangle delimits one of the windows used in the analysis (6s long, sliding 3s). *b:* The second step in the MWCS analysis: a linear regression through weighted least-squares over the time delays that have been computed during the first step. Each time-delay is associated with the mean time in its sliding window. The straight red line is the fitted slope and the dotted lines highlight the error margins.

$$\sigma_\phi^2 = \frac{\sum_j (\phi_j - m\nu_j)^2}{N-1} \tag{A.8}$$

Following Equation A.4, the time delay, δt, and its error, $e_{\delta t}$, between the two signals are taken by simply dividing m and e_m, respectively, by 2π.

Repeating this process for all windows, we obtain N_w delay-time estimates between the two cross-correlation functions, each corresponding to the central time, t_i $(i = 1, ..., N_w)$, of the window in which it was measured.

It is important to keep in mind that, for a given frequency range, $e_{\delta t}$ is inversely proportional to the square-root of the number of values that are used in the inversion. This means that if the windowed cross-correlations are zero-padded prior to Fourier transformation, the error estimate will be artificially reduced. Multiplying $e_{\delta t}$ by $\sqrt{N_{fft}}$, where N_{fft} is the number of points in the Fourier-transformed time series, removes this dependence.

A2 Velocity variation results

To a first order approximation, we can consider a stress field perturbation which acts homogeneously over the region sampled by the cross-correlated seismic noise. Under this assumption, the resulting seismic velocity perturbation $\delta v/v$ within that region will also be homogeneous, and be manifest as a stretching $-\delta t/t$ of the current cross-correlation function relative to the reference function. This stretching is constant over t, and is numerically the opposite of the velocity perturbation (Poupinet et al. 1984).

$$\frac{\delta t}{t} = -\frac{\delta v}{v} \tag{A.9}$$

Consequently, to recover $\delta v/v$, we apply a linear regression to the N_w delay-time measurements (Figure A1).

$$\delta t_i = a + bt_i \qquad , \qquad i = 1 \ldots N_w \tag{A.10}$$

where the coefficient a represents a possible instrumental drift (Stehly et al. 2007), and b corresponds to the relative time variation $\delta t/t$. Again, we can estimate these two parameters through a weighted least-squares inversion. Here, the weights, p_i, are determined using the estimated error of each time-delay measurement: $p_i = 1/e^2_{\delta t_i}$. The resulting estimate for $b = -\delta v/v$ is then

$$b = \frac{\sum p_i(t_i - \langle t \rangle)\delta t_i}{\sum p_i(t_i - \langle t \rangle)^2} \tag{A.11}$$

with variance

$$e_b^2 = \frac{1}{\sum p_i(t_i - \langle t \rangle)^2} \tag{A.12}$$

while the intercept a is

$$a = \langle \delta t \rangle - b\langle t \rangle \tag{A.13}$$

with variance

$$e_a^2 = \frac{\langle t^2 \rangle}{\sum p_i(t_i - \langle t \rangle)^2} \tag{A.14}$$

where $\langle t \rangle = \sum p_i t_i / \sum p_i$, $\langle \delta t \rangle = \sum p_i \delta t_i / \sum p_i$ and $\langle \delta t^2 \rangle = \sum p_i \delta t_i^2 / \sum p_i$ are weighted means of t, δt and t^2, respectively.

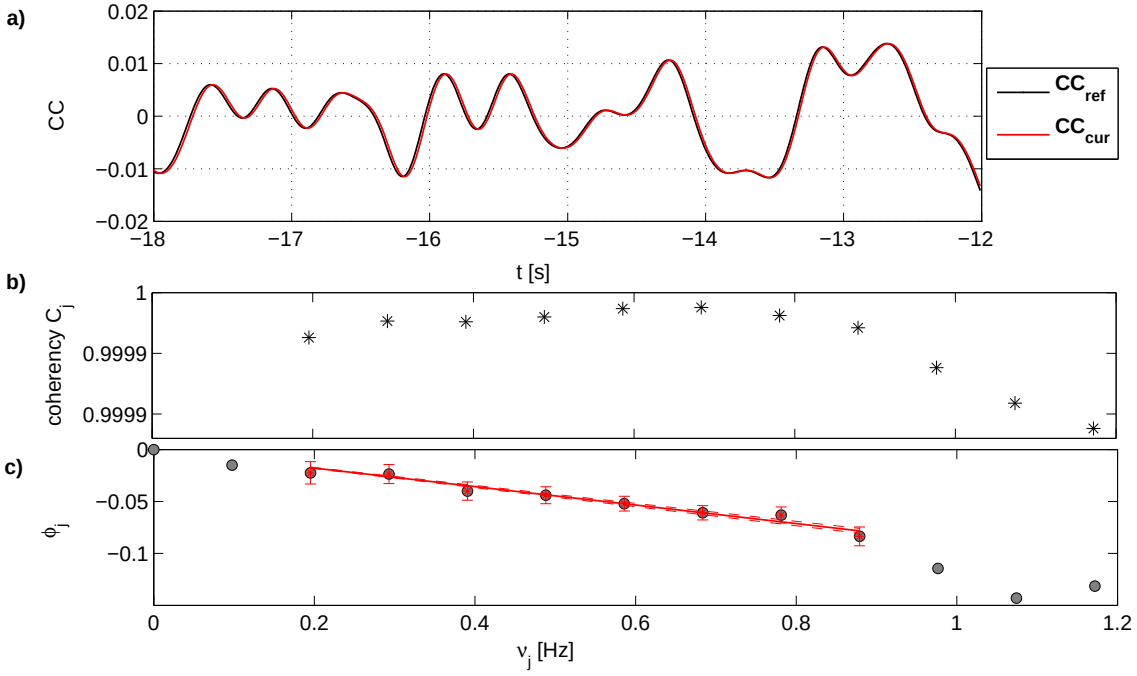

Figure A2. Example of how a delay-time is measured between two windowed cross-correlations. *a:* zoom-in of the two cross-correlations within a single lag-time window (black rectangle in Figure A1, panel a). *b:* Coherency calculated for the two windowed signals at all frequencies. *c:* Linear regression for the phase displacement along the frequencies of interest (0.2 to 0.9 Hz), which have been marked with red asterisks and errorbars ($1/w_j^2$).

An important feature of this formulation is that, for a given correlation-time interval, the error of the relative velocity variation, e_b, is inversely proportional to the square-root of the number of delay-times that are used in the regression. Consequently, if the number of sliding windows N_w is increased by reducing the time-step between consecutive windows, then the error will be artificially reduced. This is similar to the dependence of each delay time error $e_{\delta t}$ (Equation A.7) on the number of points used in the Fourier transform of the windowed data. Multiplying the estimated error by N_w is one way to remove this dependence.

APPENDIX B: DEPENDENCE OF ERRORS ON MWCS PARAMETERS

In Section 5, we observe a discrepancy (Figure 11) between the total errors we obtain from the distribution of each set of 1000 stretch estimates (e_{total}, Equation 7) and the estimated least-squares error defined by Equation A.12. One explanation for this is the dependence of the estimated error on the number of sliding windows, N_w, into which our cross-correlations are divided (see

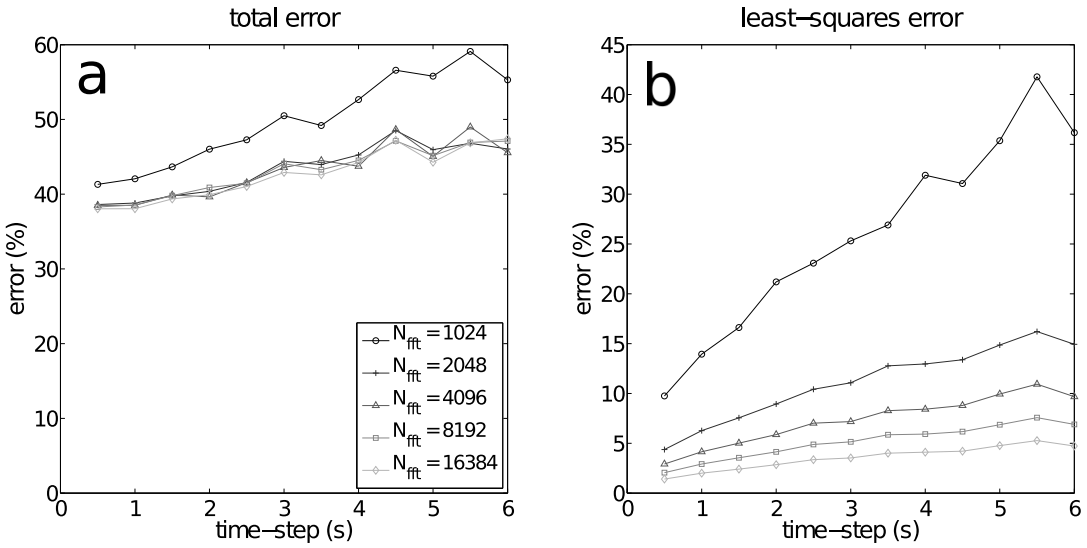

Figure A3. The dependence of $\delta t/t$ errors on N_{fft} and N_w. Total errors (*a*, Equation 7) and average least-squares errors (*b*, Equation A.12) are plotted as a function of the time-step between six-second-wide sliding windows. One curve is plotted for each value of N_{fft} (see legend). Cross-correlation functions are taken from station pair BOR–SFR. In all cases, the MWCS technique is applied 1000 times to cross-correlations that have been stretched by 0.05% and have a simulated signal to noise ratio of 5.

Appendix A2). In turn, this value is affected by the delay time errors, $e_{\delta t}$ (Equation A.7 in Appendix A1), which themselves are dependent on the number of points, N_{fft}, used to transform the windowed cross-correlations into the Fourier domain.

We observe the behaviour of the total error and the estimated error as these two parameters are varied. To this end, we alter N_w by adjusting the time-step between consecutive six-second-wide windows, and N_{fft} by zero-padding the windowed cross-correlations prior to Fourier transformation. Figure A3 shows the total error (Figure A3a) and the average least-squares error (expressed relative to $\delta t/t$, Figure A3b) we obtain when a stretch of 0.05% and a signal to noise ratio of 5 are simulated for station pair BOR–SFR. Each point corresponds to 1000 trials for a given choice of N_w and N_{fft}. These plots demonstrate the inverse proportionality between the estimated error and the square-root of both N_w and N_{fft}. Interestingly, the total error also appears to increase slightly with the time-step, suggesting that a choice of broadly overlapping windows improves the precision of the relative travel time measurements that are obtained. However, the associated error estimates must be calibrated in order to accurately evaluate the true precision of these measurements.

APPENDIX C: TEST ON THE WEIGHTS

In Section A1 we introduce weights w_j (Equation A.5) to be associated to each ϕ_j when estimating time shifts between cross-correlation functions. In this section, we test the influence of these weights on the results. In order to search for the most suitable formulation of w_j, we compare the accuracy of the yielded estimates for three different weight definitions:

$$w_j = \begin{cases} \frac{C_j^2}{1-C_j^2} & (1) \\ \frac{C_j^2}{1-C_j^2}\sqrt{|X_j|} & (2) \\ \sqrt{\frac{C_j^2}{1-C_j^2}\sqrt{|X_j|}} & (3) \end{cases}$$

Using these weights, we apply the MWCS analysis to a reference and a synthetic current function which has been perturbed from the reference by stretching it to 0.1 %. Starting from this noiseless current function, we add noise (as described in Section 4.2) to reach final signal to noise ratios of 10, 5, 2 and 1. The resulting estimates are shown in Figure A4 (a and b, respectively) for the relative error on time delay computations, and for the relative velocity variation recovered (named stretch). These measurements are in close agreement with one another, revealing only a slight dependence on the weights that are used. We choose to use $w_j(3)$ as it produces differentiated weights in cases of near constant coherence, and performs slightly better than the other schemes in these tests. Furthermore, these findings stress the importance of the noise level on the resolution of the MWCS technique as the errors shown in Figure A4 are strongly dependent on SNR values.

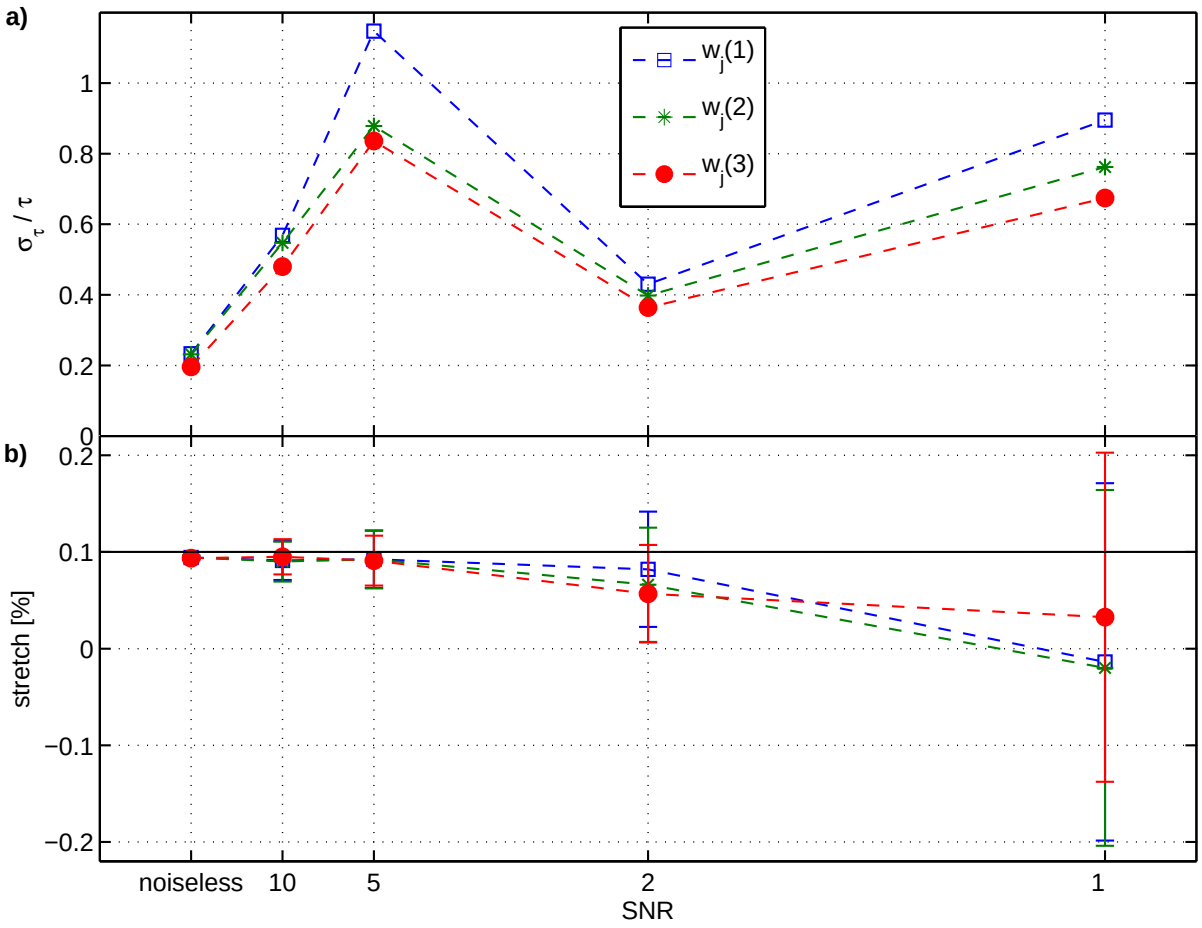

Figure A4. a) Relative error of time delay estimations versus SNR for different weights. Each symbol corresponds to one of the three definitions of w_j. b) Final results of the MWCS analysis in varying the weights and the SNR level. The symbols match those in panel a), the black horizontal line shows the real value of stretching between the two CCs.

APPENDIX D: DISTRIBUTION OF OBSERVED FLUCTUATIONS

In Section 4.2 we simulate noisy cross-correlation functions by contaminating them with a random time-series whose squared amplitude spectrum mimics that of the fluctuations we observe in real data. This time-series is drawn from a Gaussian distribution with random phase. In this section, we determine whether such a series is representative of the fluctuations that exist in real cross-correlations.

As described in Section 4.1 we observe the real fluctuations in our cross-correlations by taking the difference between corresponding current and reference functions. The cross-correlations we use in the following examples are from station pair BOR–SFR on Piton de la Fournaise volcano, and were measured during the period between 1999 and 2006.

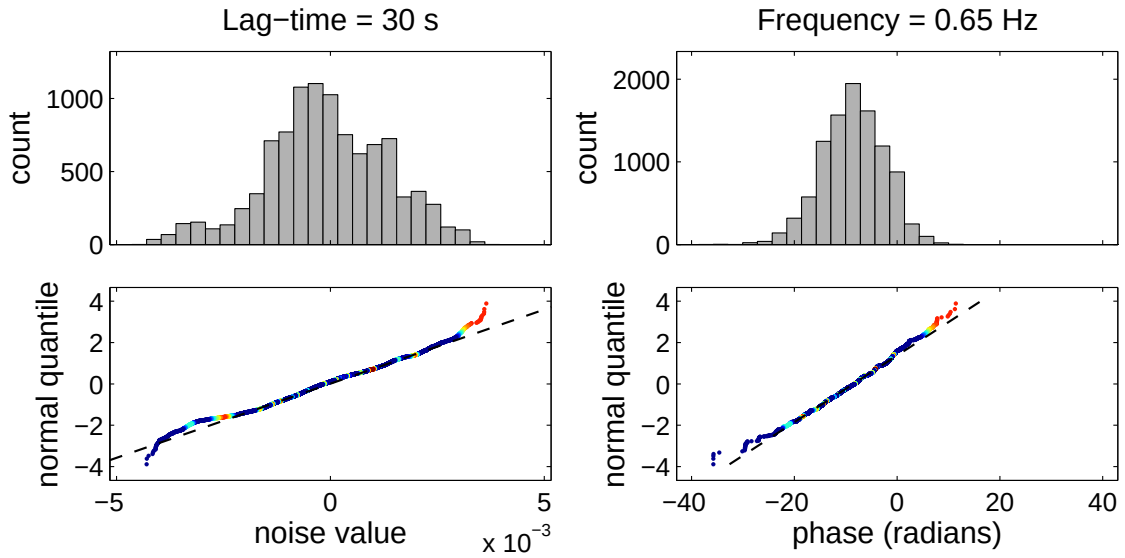

Figure A5. Distribution of the time-domain amplitude (*left*) and unwrapped phase (*right*) of the fluctuations in the current functions measured at stations BOR and SFR. A histogram (*top*) and a quantile-quantile plot (*bottom*) is shown in each case. The plotted values are coloured by the number of eruption days contained in each 30-day current stack. Colours range from blue (no eruption days) to red (30 eruption days).

We first analyze the distribution of these fluctuations in the time-domain (Figure A5, left), then consider their phase distribution (Figure A5, right) after transforming them into the Fourier domain. In both cases, we plot a histogram (top) and a quantile-quantile plot (bottom) to check for a Gaussian distribution. In this example, the time-domain distribution at 30 s lag-time, and the phase distribution at 0.65 Hz are shown. The quantile-quantile plots are made by applying the inverse normal distribution function (with zero mean and unit standard deviation) to each ranked set of measurements. The resulting series are plotted (vertical axis) against the ordered measurements (horizontal axis). As a reference, a line is plotted through the quartiles of the two series. If the plotted distribution is Gaussian, then the quantile-quantile plot should trace a straight line. Deviations from the straight line are interpreted as deviations from a Gaussian distribution.

Our tests show that the fluctuations we observe in real cross-correlations deviate slightly from a simple Gaussian distribution with random phase, mostly during eruptions. Therefore, the analysis we present in this paper relies on the fluctuations being Gaussian. One way to improve this analysis for co-eruptive periods would be to characterize the true noise distribution and randomly draw from it when simulating noisy cross-correlations. Nonetheless, the similarity between the measurement errors we observe when applying the MWCS technique to real data (Figures 4 and 5)

and those we obtain in our simulated tests (Figure 12) suggests that the methods we use to create synthetic noise and evaluate the level of fluctuation in real cross-correlations are adequate for the purposes of these tests.